CO ice mixed with CH$_3$OH: the answer to the non-detection of the 2152 cm^{-1} band?

H. M. Cuppen[1,2], E. M. Penteado[1], K. Isokoski[1], N. van der Marel[1], and H. Linnartz[1]

[1]Sackler Laboratory for Astrophysics, Leiden Observatory, Leiden University, P.O. Box 9513, 2300 RA Leiden, The Netherlands
[2]Institute for Molecules and Materials, Radboud University Nijmegen, P.O. Box 9010, 6500 GL Nijmegen, The Netherlands

13 July 2011

With this paper we provide a solution to a disagreement between astronomical and laboratory based CO-ice spectroscopic data. In observations towards icy sources, the CO-ice stretching band comprises a prominent and broad 'red component' around 2136.5 cm^{-1}. This feature is generally attributed to solid CO mixed in a hydrogen-bonded environment like H$_2$O, but, as far as we are aware, laboratory spectra have not been able to fully reproduce this feature. Water-containing CO ice cannot reproduce the observed band position and bandwidth without simultaneously producing a shoulder at 2152 cm^{-1} (4.647 μm). This band, believed to originate from the interaction of dangling-OH bonds with CO, is not observed in astronomical spectra. Fraser et al. (2004, MNRAS, 353, 59) suggested that the 2152 cm^{-1} feature is suppressed in astronomical ices by blocking of dangling-OH bonds by other species such as CO$_2$ and CH$_3$OH. In the present paper, we test this hypothesis by a systematic spectroscopic study of different H$_2$O:CO:CO$_2$ mixtures. It is shown that even though the 2152 cm^{-1} band is suppressed in low temperature spectra, the width and peak position of the red component cannot be reproduced at the same time. An ice mixture containing only CO and CH$_3$OH, however, does reproduce the spectra at low temperatures, both in terms of peak position and width of the red component and the 2152 cm^{-1} band does not appear. This indicates that CO may reside in water poor (rather than water-rich) ice in space. The astrophysical implications are discussed.

1 Introduction

The comparison of observational and laboratory infrared spectra of interstellar ices is a powerful tool to study their composition and structure. Since the shape, width and position of the absorption bands are sensitive to the molecular environment, temperature and level of energetic or chemical processing, infrared spectroscopy cannot only be exploited to obtain the overall composition of interstellar ices, but also tells us whether the ice components are mixed or layered, which separate fractions exist, and under which temperature and radiation conditions the ice was formed.

The astronomically observed CO-ice absorption feature consists of multiple components: two relatively narrow features around 2139.7 and 2143.7 cm^{-1} and a broader component around 2136.5 cm^{-1}. These components are usually referred to as the middle, blue and red component, respectively. The middle component is usually attributed to CO in an 'apolar' environment, *i.e.*, an environment

where weak van der Waals interactions dominate, like in a pure CO ice. The small blue component at 2143.7 cm^{-1} is either ascribed to mixtures of solid CO and CO$_2$ (Boogert et al. 2002; van Broekhuizen et al. 2006) or to crystalline CO ice (Pontoppidan et al. 2003b). The so-called broad (Tielens et al. 1991) or red (Pontoppidan et al. 2003b) component of the CO absorption band occurs around 2136.5 cm^{-1} and is the focus of the present work. This feature has been observed along many lines of sight (*e.g.* Tielens et al. 1991; Ehrenfreund et al. 1997; Teixeira et al. 1998; Boogert et al. 2002; Pontoppidan et al. 2003b, and references therein) and CO in a hydrogen bonding environment, like H$_2$O and CH$_3$OH containing ices, is generally considered to be responsible for the observed component (Sandford et al. 1988; Tielens et al. 1991). Since H$_2$O is the most abundant interstellar ice species, a CO:H$_2$O mixed ice is usually considered to be the carrier of the red component. A CH$_3$OH mixture with CO has previously been suggested as another possible carrier (Sandford et al. 1988; Tielens et al. 1991), but this concept has been largely ignored and has so far not been verified experimentally.

Most interstellar ice spectra are consistent with low-temperature and non-processed hydrogenated ices. The red component of the CO absorption band forms an exception to this. As mentioned earlier, this feature is generally attributed to solid CO mixed in water, but, as far as we are aware, laboratory spectra have not been able to fully reproduce this feature. The large width and red-shifted position of the CO band are only reproduced by spectra of mixed H$_2$O:CO ices with large concentrations of water (*e.g.*, Kerr et al. 1993; Chiar et al. 1994; Boogert et al. 2002). Under these circumstances the laboratory spectra show a shoulder at 2152 cm^{-1} (4.647 μm) which is not present in the observed astronomical spectra (Sandford et al. 1988; Palumbo 2006, e.g.,).

The 2152 cm^{-1} feature is associated with CO adsorbed on 'dangling-OH' bonds at the H$_2$O-ice-vacuum interface (Al-Halabi et al. 2004). 'Dangling-OH' features have been experimentally shown to disappear upon energetic processing by for instance heating (Mennella et al. 2004) or ion bombardment (Palumbo 2005). Processed ices have therefore been suggested to be responsible for the red component (Mennella et al. 2004; Palumbo 2005, 2006). However, the profiles for ice mixtures at higher temperature have a full width half maximum (FWHM) that is too small to reproduce the observational feature. Moreover, no other signatures of irradiation like the presence of OCN$^-$ or aliphatics have been seen along many of the lines of sight where the red component is detected (Pontoppidan et al. 2003b).

In the past the astronomical non-detection of the 2152 cm^{-1} feature was explained by the low spectral resolution or low signal-to-noise ratio in the observations (Ehrenfreund et al. 1997; Sandford et al. 1988) or by other overlapping features at this wavelength (Schmitt et al. 1989). However, observations by Pontoppidan et al. (2003b) showed indisputably that the 2152 cm^{-1} feature is not present in the observational spectra and stringent upper limits could be derived.

Fraser et al. (2004) have therefore tested whether a layered ice of CO and H$_2$O could explain the discrepancy between astronomical and laboratory spectra. They found that CO-H$_2$O containing interstellar ices are better represented by the evolution of a layered ice model than by a mixed ice, since a strong 2152 cm^{-1} feature would appear in the case that H$_2$O and CO are intimately mixed. When CO and H$_2$O are layered, CO only interacts with dangling-OH at the interface which suppresses the 2152 cm^{-1} feature below the detection limit. Moreover, gas-phase CO only depletes in the densest parts of interstellar clouds and solid H$_2$O has been observed in regions where CO was still in the gas phase. However, a purely layered model cannot explain the presence of the red component and Fraser et al. (2004) suggested that a small fraction of CO diffuses into the H$_2$O component, which would in turn lead to a schouder at 2152 cm^{-1}. They further proposed that this feature is suppressed in astronomical spectra by blocking of the dangling-OH by other species such as CO$_2$ and CH$_3$OH. In the present paper, we test this hypothesis by a systematic spectroscopic study of different H$_2$O:CO:CO$_2$ mixtures and we show that although the 2152 cm^{-1} band can be suppressed in low temperature spectra, the width and peak position of the red component cannot be reproduced at the same time.

A mixture of CO and CH$_3$OH, however, reproduces the astronomical spectra, *i.e.*, the laboratory features match the astronomically observed red component data and the 2152 cm^{-1} feature does not show up. This is consistent with a number of recent findings. Laboratory experiments show that CH$_3$OH can be formed on icy grains from CO (Watanabe et al. 2004; Fuchs et al. 2009) and model simulations of CH$_3$OH formation in dense cores indeed result in grain mantles with CO and

CH_3OH intimately mixed (Cuppen et al. 2009). Bottinelli et al. (2010) recently showed for *Spitzer* observations of solid methanol lines that the methanol profiles are consistent with $CH_3OH:CO = 1:1$ mixtures. Although, a separate CH_3OH-rich and H_2O-poor component fit the observations as well.

The present paper is structured as follows. Section 2 presents the experimental procedure for obtaining the laboratory spectra. Section 3 gives the fitting procedure used to extract the spectral characteristics from observed CO ice absorption bands. Section 4 tests the hypothesis of the suppression of the 2152 cm^{-1} band by CO_2 and Section 5 extends this to the case of methanol and discusses $CO:CH_3OH$ mixtures as carriers for the red component at 2136.5 cm^{-1}. Section 6 concludes and gives the astrophysical implications of this work.

2 Experimental procedure

All experiments are performed in a high vacuum (HV) setup, which has a base pressure of 5×10^{-7} mbar at room temperature and is described in detail by Gerakines et al. (1995) and Bouwman et al. (2007). In short, the CsI sample window is cooled to 15 K by a closed-cycle helium cryostat and the samples are then deposited from the gas phase on the window with the direction along the surface normal. To enable a direct comparison of the spectra obtained for the different ice mixtures, the amount of deposited H_2O and CH_3OH is kept constant at 3000 ML for $H_2O:CO:CO_2$ and $CH_3OH:CO$ mixtures, respectively.

Transmission Fourier transform infrared spectra of the ice mixtures are recorded in a single pass with a Bio-Rad 40-A spectrometer and a Varian 670-IR FTIR spectrometer for the $H_2O:CO:CO_2$ and $CH_3OH:CO$ mixtures, respectively. Spectra are taken between 4000-400 cm^{-1} (2.5-25 μm) with a resolution of 1 cm^{-1} using a total of 256 scans per spectrum to increase the SNR. The spectrometer is flushed with dry air to minimise background fluctuations due to atmospheric absorptions. Background spectra are acquired prior to deposition for each experiment. Each sample is measured at fixed temperatures between 15 and 135 K, at 15, 22, 25, 30, 45, 60, 75, 90, 105 and 135 K. The sample is heated with a resistive heater, using a Lakeshore temperature controller unit. The temperature is measured by a silicon diode. After each heating step, the sample is allowed to stabilise for two minutes.

The gas mixtures are prepared separately in a glass vacuum line with a base pressure of 10^{-5} mbar. The gases CO (Praxair, 99.999% purity for $H_2O:CO:CO_2$ mixtures and Linde, 99.997% for $CH_3OH:CO$) and CO_2 (Praxair, 99.98% purity) are directly used from the high pressure gas bottle, whereas deionised H_2O and CH_3OH (Sigma-Aldrich, 99.9% purity) are further purified by three freeze-pump-thaw cycles. In the present study, the following mixtures are used: $CH_3OH:CO = 9:1, 4:1, 2:1, 1:1, 1:2, 1:4$ and $1:9$ and $H_2O:(CO+CO_2) = 4:1, 2:1, 1:1, 1:2$ and $1:4$ for each $H_2O:(CO+CO_2)$ ratio five different $CO:CO_2$ ratios. Figure 1 shows a selection of spectra at 15 K for different mixtures. The $H_2O:CO$ spectrum is taken from Bouwman et al. (2007). A pure CO ice has an absorption band at 2139.7 cm^{-1} (4.65 μm) (dash-dotted curve) (Ehrenfreund et al. 1997). All spectra are normalised to the maximum of this feature. Figure 1 clearly shows the broadening of the band by the presence of other constituents in the ice as well as the appearance of the shoulder at 2152 cm^{-1}. All features have a line shape that is close to a Gaussian. The peak position and presence of the shoulder at 2152 cm^{-1} is highly dependent on the exact composition of the ice mixture. In the next paragraphs we will extract characteristics such as width, peak position and presence of the 2152 cm^{-1} shoulder from the experimental spectra and compare these to the characteristics of astronomically observed CO ice spectra.

3 Observations of the red component

Pontoppidan et al. (2003b) performed a Very Large Telescope (VLT) spectroscopic survey of 39 Young Stellar Objects (YSOs) with high signal to noise ratio and high spectral resolution. We use this data to extract information about the red component in astronomical observations and compare this to laboratory spectra. For this a phenomenological approach is used that has the advantage that spectral characteristics can be compared to a wide range of different experimental data. Another method that
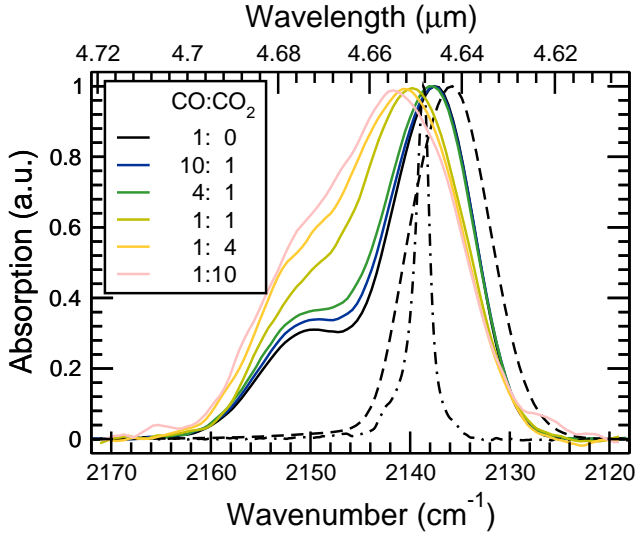
Figure 1: Experimental spectra of CO absorption band in $H_2O:CO:CO_2$ mixtures (solid curves) and $CH_3OH:CO = 1:1$ mixture (dashed curve) at 15 K. The $H_2O:CO:CO_2$ mixtures have a ratio of $H_2O:(CO+CO_2) = 4:1$ and different $CO:CO_2$ ratios as indicated in the legend. A pure CO spectrum is shown by the dash-dotted curve.

is often adopted is the so-called mix-and-match approach, in which observational spectra are fitted with a small selection of experimental templates of typical ice mixtures. However, often a degeneracy exists between laboratory spectra recorded under different experimental conditions.

Our phenomenological approach is more geared towards a comparison with the experimental data. For instance, Pontoppidan et al. (2003b) used a Lorentzian line shape to fit the red component and two Gaussians for the blue and middle components, since this would better describe the observational results. They argued that a Lorentzian shape may be a better representation of IR band profiles of CO in an environment which is dominated by weak van der Waals interactions. The blue and middle components have a high CO content, since they are most likely due to a $CO:CO_2$-ice or crystalline CO ice and a CO-dominated ice, respectively. Because of the high CO content, grain shape effects are important and these could distort the Lorentzian profile to emulate Gaussian line shapes. We however obtain better fits of both the experimental and observational spectra by using Gaussians for all three components as can be seen in Fig. 2. Since the red component is most likely caused by CO in a hydrogen bonding environment, we argue that the simple model of Lorentz oscillators breaks down for this component. This is an additional argument to use a Gaussian line shape for our fits.

In addition to the three CO components, some observational spectra show a band around 2175 cm^{-1}, which can be attributed to the stretching mode of CN bonds. The most likely carrier for this bond is OCN^- (Schutte & Greenberg 1997; Pendleton et al. 1999; Novozamsky et al. 2001). This extra component is fitted with a Gaussian as well.

The following fitting procedure has been applied to all spectra. Four Gaussians are fitted to the data in the 2185-2120 cm^{-1} range. The peak positions are free for all components. The FWHM is only allowed to vary for the 2175 cm^{-1} feature, similar to the fitting procedure of Pontoppidan et al. (2003b). The FWHM of the blue and middle components are also take from this work as 3.0 and 3.5 cm^{-1}, respectively. Since the width of the red feature is sensitive to the exact composition of the polar ice, 56 independent fits are performed for each spectrum in which this FWHM is fixed by 56 different values between 3 and 14 cm^{-1}. The final sum-of-squares errors as a function of FWHM determine the best value of the FWHM and its uncertainty (error within 1% of best value). The uncertainty in the peak position is taken from the spread obtained in the fits within the FWHM range. Figure 3 shows an example of a fitted observational spectrum. Here the spectrum of Elias 32 is shown which has an average FWHM (8.9 ± 0.7 cm^{-1}) and peak position (2136.7 ± 2.4 cm^{-1}) for the red component.

Figure 4 plots the results for all fits. Outcomes with a small red contribution are excluded from this
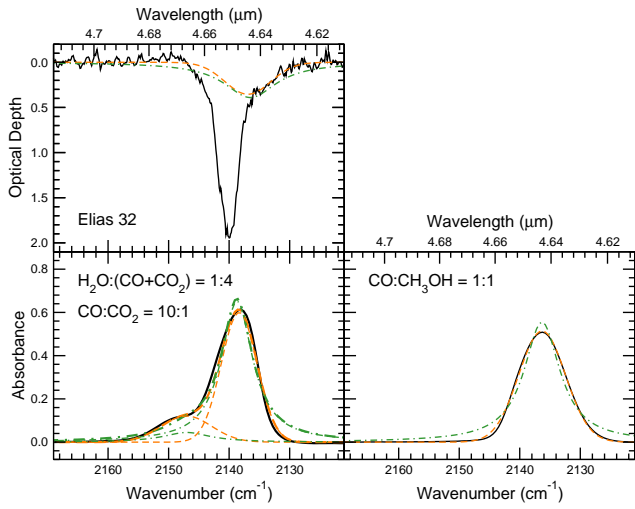
4

Figure 2: A comparison between fits of the red CO-ice profile by Gaussian lineshapes (dashed curves) and by Lorentzian lineshapes (dash-dotted). (Top) The Gaussian fit yields the best-fit result for Elias 32 and is used in this study; the Lorentzian result is taken from Pontoppidan et al. (2003b).
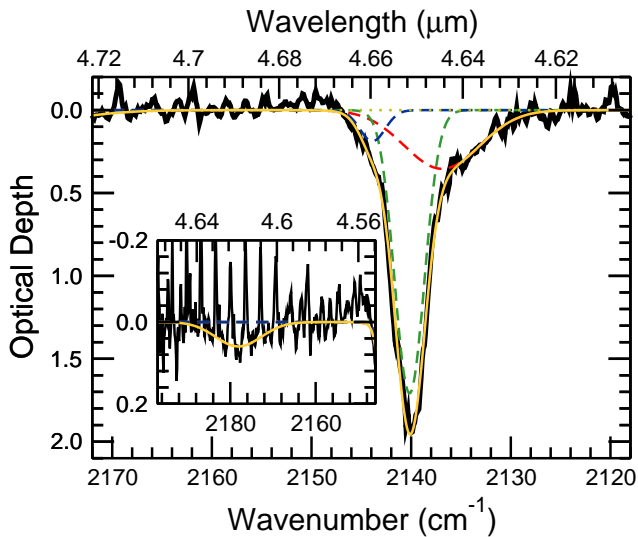

Figure 3: The observational spectra, here Elias 32, are fitted by four Gaussians representing the red (FWHM = 8.9 cm^{-1}), middle, and blue component and the 2175 cm^{-1} band (shown in the inset and likely due to OCN$^-$).
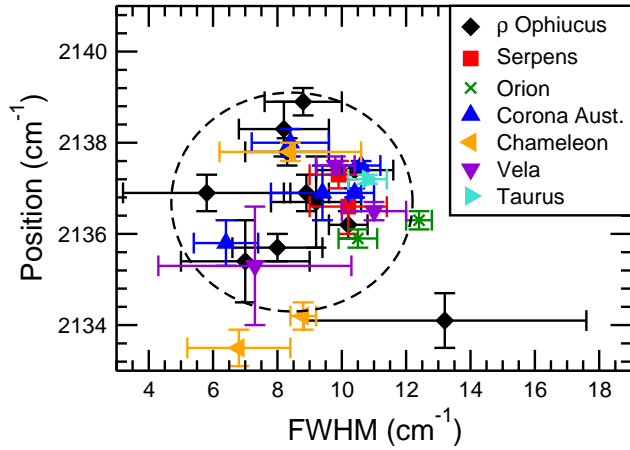
Figure 4: The spread in FWHM and position of the red component in the observational spectra (Pontoppidan et al. 2003b). The circle serves as a guide to the eye.

plot. Most objects lie in the circle 8.5 ± 3.8 cm^{-1} and 2136.7 ± 2.4 cm^{-1} which serves as a guide to the eye and will later be used to compare to the experimental data. The circle is based on the median value of the position and FWHM and 3 times the median absolute deviation. The median position is in close agreement with Pontoppidan et al. (2003b) who obtained 2136.5 cm^{-1}, whereas the present FWHM value of 8.5 cm^{-1} is smaller than the value of 10.6 cm^{-1} found Pontoppidan et al. (2003b), even though this was for a Lorentzian instead of a Gaussian profile.

As mentioned before, none of the observational spectra shows a 2152 cm^{-1} feature. Pontoppidan et al. (2003b) obtained lower limits on the ratio between the red component at $\sim$2136.5 cm^{-1} and the 2152 cm^{-1} dangling-OH band for the highest quality interstellar spectra. For most sources these limits fall between 6 and 9 as plotted in their Fig. 21, but several sources have even higher lower limits. In order to explain the observational spectra, laboratory spectra should have a CO-2136/CO-2152 ratio of at least 6 and a FWHM and peak position of the main band that is in agreement with 8.5 ± 3.8 cm^{-1} and 2136.7 ± 2.4 cm^{-1}. Since CO is probably only a minor species in the ice mixture responsible for the observed 2136.5 cm^{-1} feature, grain shape effects are assumed to be minimal and the observational data and laboratory data can be directly compared.

4 Dangling-OH blocking by CO$_2$

As mentioned in the introduction, one of the suggestions for the astronomical non-detection of the 2152 cm^{-1} is blocking of the dangling-OH site of water by other molecules in the interstellar ice. Since one of the other main ice components, besides H$_2$O and CO, is CO$_2$, this species was proposed as a potential candidate (Fraser et al. 2004). Since this hypothesis has not been tested by laboratory experiments yet, we performed a systematic spectroscopic study of H$_2$O:CO:CO$_2$ mixtures and compared their spectral characteristics to the observed spectra. Spectra of 25 different H$_2$O:CO:CO$_2$ mixtures at ten different temperatures between 15 and 135 K were recorded. As explained in Section 2, the different mixing ratios are given by H$_2$O:(CO+CO$_2$) = 4:1, 2:1, 1:1, 1:2 and 1:4 with CO:CO$_2$ = 10:1, 4:1, 1:1, 1:4, and 1:10 for each combination. Each of the thus-obtained 250 spectra is fitted by two Gaussians: one representing the 2152 cm^{-1} feature and one the main feature between 2136.5 and 2139 cm^{-1}.

Figure 5 shows a limited set of the spectra (45 out of 250 spectra) to illustrate the effect of ice composition and temperature on the CO absorption feature, together with the fitted Gaussians. Again all spectra are normalised to maximum of the CO feature. The most differing mixtures are used and the lower temperatures have been selected. At higher temperatures a large fraction of CO has desorbed. The individual panels clearly show that the CO profile is strongly affected by the presence of CO$_2$ and H$_2$O. In general, the presence of H$_2$O and CO$_2$ appears to have orthogonal effects: more H$_2$O leads to a red-shift and an increase of the 2152 cm^{-1} feature, whereas more CO$_2$ leads to a blue-shift and

a suppression of the 2152 cm^{-1} feature.

The fitted Gaussians are used for the comparison with the observations. The main Gaussian is compared to the red component and the ratio between the optical depths between the CO-main and CO-2152 is compared to the lower limit of the CO-2136/CO-2152 ratio that was observationally determined. Since not all experimental spectra have a feature peaking at 2136.5 cm^{-1}, the main CO feature is used instead. At a later stage we will consider the exact band position of the main feature and the spectra that do not reproduce the astronomically observed position are excluded in that process.

For five mixing ratios a CO-main/CO-2152 larger than 6 was found at low temperatures. Four of these mixing ratios fulfil H$_2$O:(CO+CO$_2$) = 1:4 or 1:2 and CO:CO$_2$ = 1:4 or 1:10 and the fifth mixing ratio is H$_2$O:CO:CO$_2$ = 25:90:9 (H$_2$O:(CO+CO$_2$) = 1:4 and CO:CO$_2$ = 10:1). The latter only just fulfills the CO-main/CO-2152 > 6 criterion and only for three low temperatures: 22, 25 and 30 K as can be seen in Fig. 5. Other compositions reach CO-main/CO-2152 ratios larger than 6 at elevated ice temperatures ($T > 60$ K) well above the CO desorption temperature (Öberg et al. 2005, $T \sim 28$ K). The top panel of Figure 6 plots the position and FWHM of the spectra of the first five mixing ratios at different temperatures. A series of identical symbols reflects the same mixing ratio but for different temperatures, as annotated below each symbol. The circle in this panel is the same circle as plotted in Figure 4 and is drawn to simplify the visual comparison between observations and experiments. One can clearly see that the observed combination of position and FWHM is only obtained for a few spectra. These spectra are for H$_2$O:CO:CO$_2$ = 25:90:9, which has a CO-main/CO-2152 ratio only just above the threshold value of 6, whereas the astronomical limits are often much higher, and only covers a region at the edge of the circle. This ice combination can therefore not represent the majority of the astronomically observed red CO-ice components.

Summarising, one can conclude that the addition of CO$_2$ to a H$_2$O:CO mixture can indeed reduce the dangling-OH leading to the disappearance of the 2152 cm^{-1} at low temperatures, but this requires such large quantities of CO$_2$ that H$_2$O is no longer the major ice species and the position and width of the main feature no longer agrees with the characteristics of the astronomically observed features. The width and position resemble in this case better a CO:CO$_2$ ice. Mixtures with smaller fractions of CO$_2$ reproduce the width and position, but also show substantial shoulders at 2152 cm^{-1}. The addition of CO$_2$ can therefore not explain the observed spectral features of the red component of the CO absorption band.

5 CO mixed with CH$_3$OH

The present section tests whether a mixture of CO with CH$_3$OH can explain the observed characteristics. As far as we are aware, spectroscopy on unprocessed CO and CH$_3$OH containing mixtures has not been directly linked to the 2136 cm^{-1} component (Palumbo & Strazzulla 1993) or has only been performed in the presence of H$_2$O causing a shoulder at 2152 cm^{-1} (Sandford et al. 1988; Hudgins et al. 1993), except in Bisschop (2007). Here we investigate CO solely mixed with CH$_3$OH. Recent observations of solid CH$_3$OH (Boogert et al. 2008) showed that CH$_3$OH is most likely present in a water-poor environment and that a mixture of CO:CH$_3$OH is consistent with the observed width and position of the methanol band (Bottinelli et al. 2010). Furthermore, since CO is a precursor of CH$_3$OH through H-atom addition reactions (Watanabe et al. 2004; Fuchs et al. 2009), they are likely to be present in the same ice component on the grains.

The dashed curve in Figure 1 plots the CO absorption band for CO:CH$_3$OH = 1:1 mixture at 15 K. It shows that the addition of CH$_3$OH results in a broad, red-shifted peak without a shoulder at 2152 cm^{-1}. The seven ice compositions used in present work (CO:CH$_3$OH = 9:1, 4:1, 2:1, 1:1, 1:2, 1:4 and 1:9) cover a large range in mixing ratios and the spectra do not exhibit a shoulder at 2152 cm^{-1} as can be seen in Fig. 7. This figure gives an overview of the CO band profile in a CH$_3$OH-environment for different mixing ratios and temperatures. The figures shows that the feature become more redshifted and wider with CH$_3$OH-content. These spectra are again fitted to extract the spectral characteristics. In this case a single Gaussian is used, because of the absence of the shoulder at 2152 cm^{-1}. The resulting fits are plotted in gray with a dashed curve and overlap with the data in most cases. The
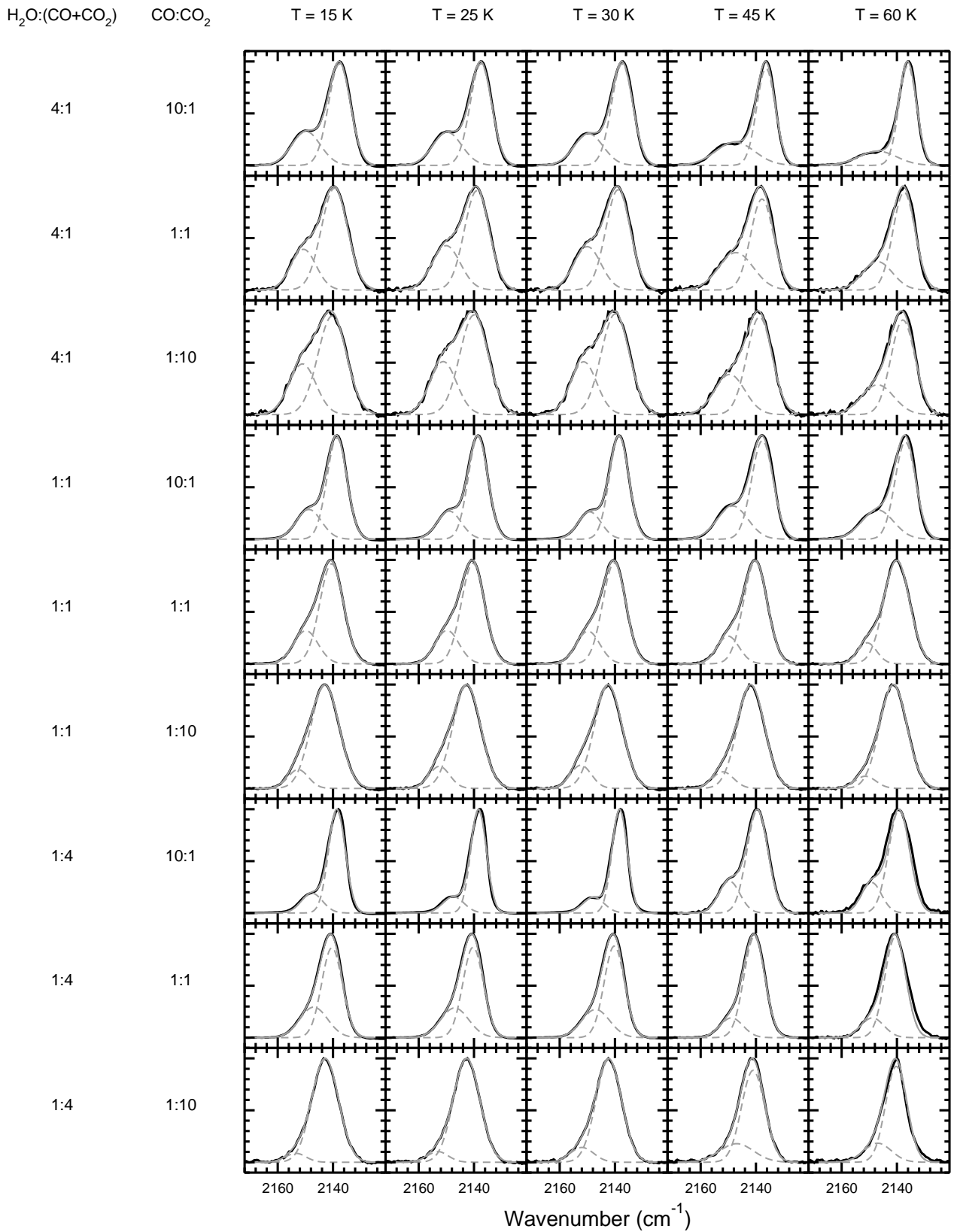
Figure 5: A limited set of CO profiles for different H_2O:CO:CO_2 mixtures at different temperatures, to illustrate how the CO profile — width, position and presence of the 2152 cm^{-1} feature — changes with composition and temperature. All ices are deposited at 15 K and then subsequently heated to measure the higher temperatures. Spectra are normalised to the maximum of the CO feature.
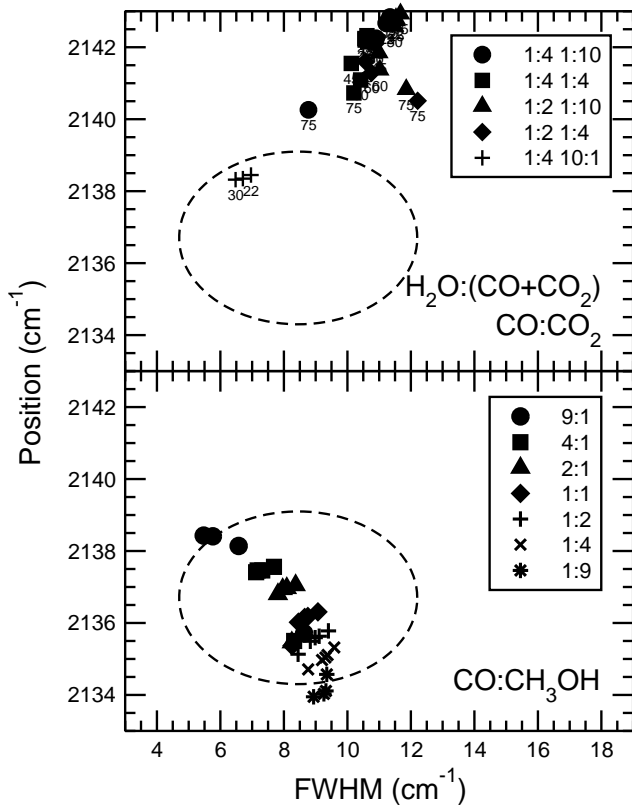
Figure 6: The FWHM and position of the CO absorption band in laboratory spectra of a range of different $H_2O:CO:CO_2$ (top panel) and $CH_3OH:CO$ (bottom panel) ice mixtures at different temperatures. The circles serve as a guide to the eye to allow easy comparison to the observational data in Figure 4.
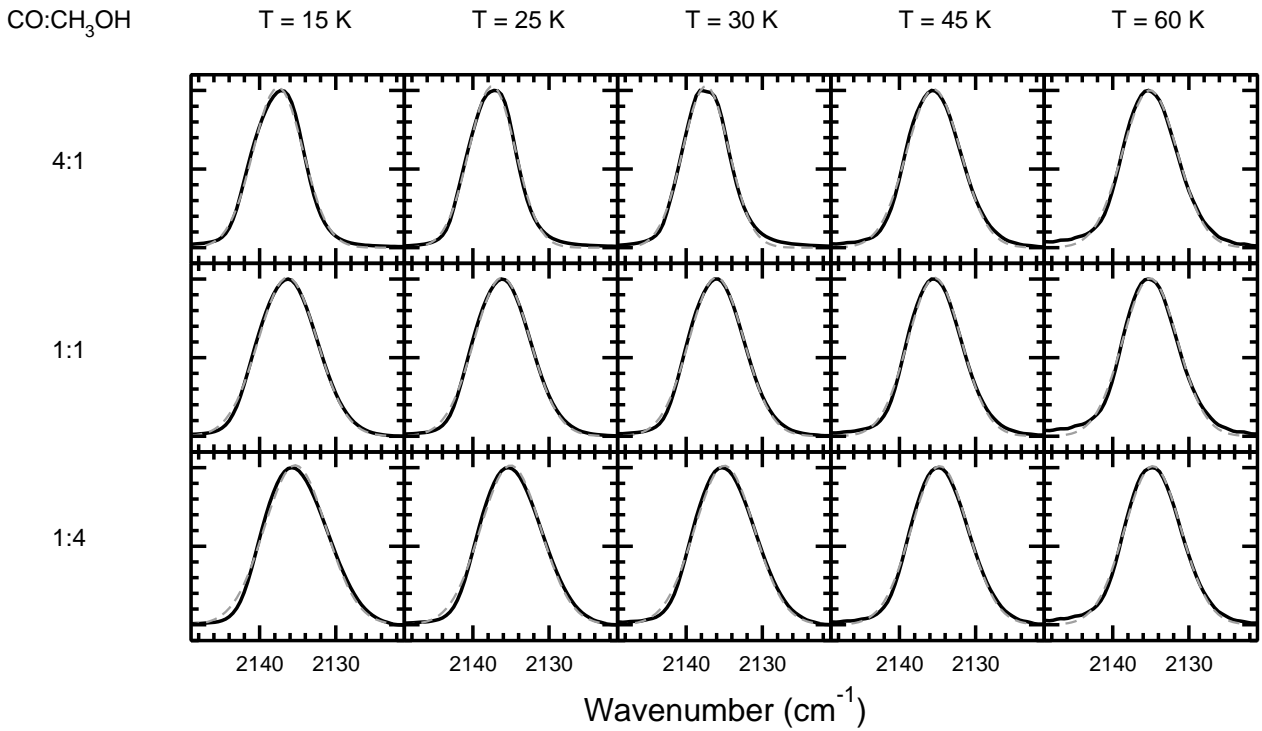

Figure 7: Similar to Fig. 5 for $CO:CH_3OH$ ice mixtures.

Table 1: The peak position and FWHM for different CO:CH$_3$OH ice mixtures and temperatures.

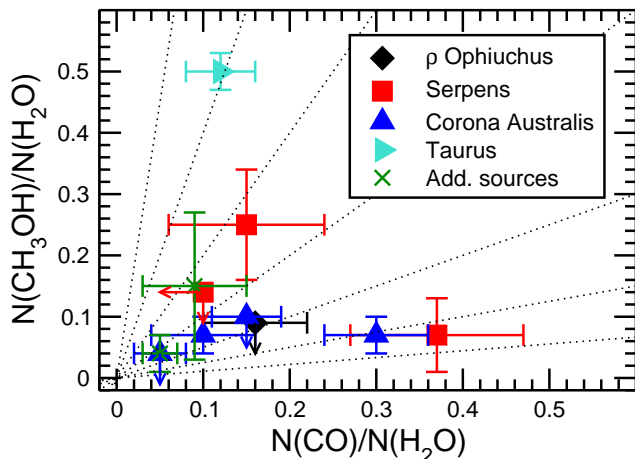| CO:CH$_3$OH	position (cm^{-1})				FWHM (cm^{-1})			
	15 K	25 K	30 K	45 K	15 K	25 K	30 K	45 K
1:9	2134.6	2134.1	2134.0	2133.9	9.35	9.32	9.26	8.94
1:4	2135.3	2135.0	2135.0	2134.7	9.59	9.30	9.20	8.76
1:2	2135.8	2135.6	2135.5	2135.1	9.40	8.98	8.83	8.45
1:1	2136.3	2136.1	2136.0	2135.4	9.07	8.65	8.46	8.26
2:1	2137.0	2136.9	2136.8	2135.5	8.37	7.96	7.81	8.25
4:1	2137.6	2137.5	2137.4	2135.5	7.69	7.17	7.12	8.32
9:1	2138.1	2138.4	2138.4	2135.7	6.57	5.76	5.47	8.64

Figure 8: The observed column densities of polar CO versus CH$_3$OH w.r.t. H$_2$O ice. The dotted lines indicate different mixing ratios (9:1, 4:1, 2:1, 1;1, 1:2, 1:4, 1:9).

corresponding positions and FWHMs are given in Table 1.

The bottom panel of Figure 6 plots the FWHM versus the position of the CO absorption band for different CO:CH$_3$OH mixing ratios at different temperatures between 15 and 45 K. The circle that marks the observational range is now clearly filled. Moreover, mainly the low temperature spectra fall in the circle. The exact position in the circle depends on the mixing ratio of CO and CH$_3$OH. Ratios between 1:9 and 9:1 are within the boundaries defined by the circle and reproduce the spectral characteristics of the observations. The majority of the observational spectra are best reproduced by ratios between CO:CH$_3$OH=1:2 and 4:1.

The ratios based on spectral characteristics are indeed consistent with interstellar CO:CH$_3$OH ice ratios based on observed ice abundances as can be seen from Figure 8. This graph shows the 'polar' CO abundance with respect to water ice derived from the red component versus the solid CH$_3$OH abundance. Column densities for polar CO are taken from Pontoppidan et al. (2003b) and for H$_2$O and CH$_3$OH ice from Boogert et al. (2008). The error bars represent 3 σ limits. The dotted lines indicate the different mixing ratios as studied experimentally: from CO:CH$_3$OH=1:9 (top left) to 9:1 (bottom right). The two additional sources are W33A and GL 2136. The figure shows that based on the column densities most observational ratios fall between CO:CH$_3$OH = 1:2 and 4:1, which is in close agreement with the conclusions based on the spectral characteristics. Note that for large CO:CH$_3$OH ratios, grain shape effects can have an influence on the observed spectra and the experimental spectra should be adjusted for this. Since the optical constants are not available for the measured spectra, this effect is ignored for the moment in this comparison.

6 Conclusions and astrophysical implications

The combined astronomical and laboratory data discussed in the present paper show, that the red component of the CO absorption band can be explained by a mixture of solid CO and CH_3OH without the presence of H_2O. Previously considered water-containing mixtures resulted in the appearance of a shoulder at 2152 cm^{-1} in laboratory spectra, which posed a problem, since this feature is not observed astronomically. The discrepancy is solved in the present paper by considering a water-poor mixture. It is credible that other species, chemically related to CH_3OH, are able to reproduce this result as well, but given the direct relation between CO and CH_3OH, methanol is a very likely candidate.

This provides additional proof that CO only freezes out after H_2O has formed on the grain, leading to at least two separate ice components: a H_2O-rich and a CO-rich layer. Observational studies already showed that CO mainly freezes out in the centres of dense cold cloud cores (Pontoppidan 2006; Pontoppidan et al. 2008) where most of the gas is in molecular form and H_2 and CO are the dominant species. In these centres, most of the elemental oxygen is in the form of CO or frozen out onto grains in form of H_2O.

The spectral characteristics of the red component require a high fraction of CH_3OH to be present. This means that almost all CH_3OH is present in the CO:CH_3OH component. This is in general agreement with observations of solid CH_3OH. It is hard to constrain the percentage of CH_3OH mixed with water observationally, since the 9.75 μm band profile of CH_3OH hardly changes with ice composition, neither in peak shape nor position. The feature only becomes red-shifted when water ice is dominant, *i.e.*, >90% (Bottinelli et al. 2010; Skinner et al. 1992). The 3.54 μm CH_3OH feature can also be applied to constrain the CH_3OH ice environment (Dartois et al. 1999; Pontoppidan et al. 2003a; Thi et al. 2006). All of these studies generally conclude that at least a fraction of the CH_3OH ice is in a water-poor, CH_3OH-rich environment.

The observation that CH_3OH is predominantly mixed with CO in a H_2O-poor environment leads to the conclusion that CH_3OH is mainly formed through hydrogenation of CO (Watanabe et al. 2004; Fuchs et al. 2009) and not by for instance UV or ion processing of a H_2O containing ice (Hudson & Moore 1999). Grain surface chemistry simulations of CO in a water-poor environment indeed showed that CH_3OH can be formed in this way and that CH_3OH is mainly present on the grain mantles in the pure form or mixed with CO, and that it is not in a water-rich phase (Cuppen et al. 2009).

The presence of separate H_2O-rich and CO/CH_3OH-rich ice fractions has to be taken into account by modellers and experimentalists. In models, often H_2O and CH_3OH are formed simultaneously, since gas phase CO and O are simultaneously deposited. Here we have shown that the subsequent formation of H_2O and CH_3OH is more likely. This should be reflected in the modelled conditions. The same holds for ice experiments, where often CO:H_2O or CH_3OH:H_2O mixtures are used to represent typical interstellar ices. The present study shows again that not all species are intimately mixed in the ice and that the composition of astrophysically relevant ice mixtures should therefore be treated with care.

7 Acknowledgements

References

Al-Halabi A., Fraser H. J., Kroes G. J., van Dishoeck E. F., 2004, A&A, 422, 777

Bisschop S. E., 2007, PhD thesis, Leiden Observatory, Leiden University

Boogert A. C. A., Hogerheijde M. R., Blake G. A., 2002, ApJ, 568, 761

Boogert A. C. A., Pontoppidan K. M., Knez C., et al.,2008, ApJ, 678, 985

Bottinelli S., Adwin Boogert A. C., Bouwman J., Beckwith M., van Dishoeck E. F., Öberg K. I., Pontoppidan K. M., Linnartz H., Blake G. A., Evans N. J., Lahuis F., 2010, ApJ, 718, 1100

Bouwman J., Ludwig W., Awad Z., Öberg K. I., Fuchs G. W., van Dishoeck E. F., Linnartz H., 2007, A&A, 476, 995

Chiar J. E., Adamson A. J., Kerr T. H., Whittet D. C. B., 1994, ApJ, 426, 240

Cuppen H. M., van Dishoeck E. F., Herbst E., Tielens A. G. G. M., 2009, A&A, 508, 275

Dartois E., Schutte W., Geballe T. R., Demyk K., Ehrenfreund P., D'Hendecourt L., 1999, A&A, 342, L32

Ehrenfreund P., Boogert A. C. A., Gerakines P. A., Tielens A. G. G. M., van Dishoeck E. F., 1997, A&A, 328, 649

Fraser H. J., Collings M. P., Dever J. W., McCoustra M. R. S., 2004, MNRAS, 353, 59

Fuchs G. W., Cuppen H. M., Ioppolo S., Romanzin C., Bisschop S. E., Andersson S., van Dishoeck E. F., Linnartz H., 2009, A&A, 505, 629

Gerakines P. A., Schutte W. A., Greenberg J. M., van Dishoeck E. F., 1995, A&A, 296, 810

Hudgins D. M., Sandford S. A., Allamandola L. J., Tielens A. G. G. M., 1993, ApJS, 86, 713

Hudson R. L., Moore M. H., 1999, Icarus, 140, 451

Kerr T. H., Adamson A. J., Whittet D. C. B., 1993, MNRAS, 262, 1047

Mennella V., Palumbo M. E., Baratta G. A., 2004, ApJ, 615, 1073

Novozamsky J. H., Schutte W. A., Keane J. V., 2001, A&A, 379, 588

Öberg K. I., van Broekhuizen F., Fraser H. J., Bisschop S. E., van Dishoeck E. F., Schlemmer S., 2005, ApJ, 621, L33

Palumbo M. E., 2005, J. Phys. Conf. Series, 6, 211

Palumbo M. E., 2006, A&A, 453, 903

Palumbo M. E., Strazzulla G., 1993, A&A, 269, 568

Pendleton Y. J., Tielens A. G. G. M., Tokunaga A. T., Bernstein M. P., 1999, ApJ, 513, 294

Pontoppidan K. M., 2006, A&A, 453, L47

Pontoppidan K. M., Boogert A. C. A., Fraser H. J., van Dishoeck E. F., Blake G. A., Lahuis F., Öberg K. I., Evans II N. J., Salyk C., 2008, ApJ, 678, 1005

Pontoppidan K. M., Dartois E., van Dishoeck E. F., Thi W.-F., d'Hendecourt L., 2003a, A&A, 404, L17

Pontoppidan K. M., Fraser H. J., Dartois E., Thi W., van Dishoeck E. F., Boogert A. C. A., d'Hendecourt L., Tielens A. G. G. M., Bisschop S. E., 2003b, A&A, 408, 981

Sandford S. A., Allamandola L. J., Tielens A. G. G. M., Valero G. J., 1988, ApJ, 329, 498

Schmitt B., Greenberg J. M., Grim R. J. A., 1989, ApJ, 340, L33

Schutte W. A., Greenberg J. M., 1997, A&A, 317, L43

Skinner C. J., Tielens A. G. G. M., Barlow M. J., Justtanont K., 1992, ApJ, 399, L79

Teixeira T. C., Emerson J. P., Palumbo M. E., 1998, A&A, 330, 711

Thi W.-F., van Dishoeck E. F., Dartois E., Pontoppidan K. M., Schutte W. A., Ehrenfreund P., D'Hendecourt L., Fraser H. J., 2006, A&A, 449, 251

Tielens A. G. G. M., Tokunaga A. T., Geballe T. R., Baas F., 1991, ApJ, 381, 181

van Broekhuizen F. A., Groot I. M. N., Fraser H. J., van Dishoeck E. F., Schlemmer S., 2006, A&A, 451, 723

Watanabe N., Nagaoka A., Shiraki T., Kouchi A., 2004, ApJ, 616, 638